SIMULATION OF OSCILLATING ARM WIRE MONITOR MECHANICS DRIVEN BY A STEPPER MOTOR

R. Dölling[†], Paul Scherrer Institut, Villigen, Switzerland

Abstract

The present oscillating arm wire monitors at HIPA operate with wire speeds of 0.75 m/s. Based on basic dynamic simulations of mechanics and motor, we discuss possible variants of this design using stepper motors in open loop control. The results suggest that 4 m/s can be reached with sufficient position resolution, when using a predefined step sequence customized to the mechanics. This speed should be sufficient to measure the full proton beam current in the injection line.

INTRODUCTION

The majority of profile monitors presently operating in the 0.87 MeV, 72 MeV and 590 MeV beam lines of HIPA are wire monitors using an oscillating monitor arm (MA). A fork at the MA holds the wire, foil, or finger, which is moved transversely through the beam (Fig. 1) [1, 2]. The MA is driven via a con-rod (CR) from a crank wheel (CW), which again is driven via a gear (MG) connected to a brushed DC motor. A bellow at the MA axis of rotation separates the vacuum from the in-air mechanics. Since the bellow needs to bend only ±10°, its lifetime is practically unlimited at the given maximum wire speed of 0.75 m/s. The wire position is determined by a potentiometer attached to the MA, while the home position is indicated by a home switch (HS) actuated by a cam on the CW.
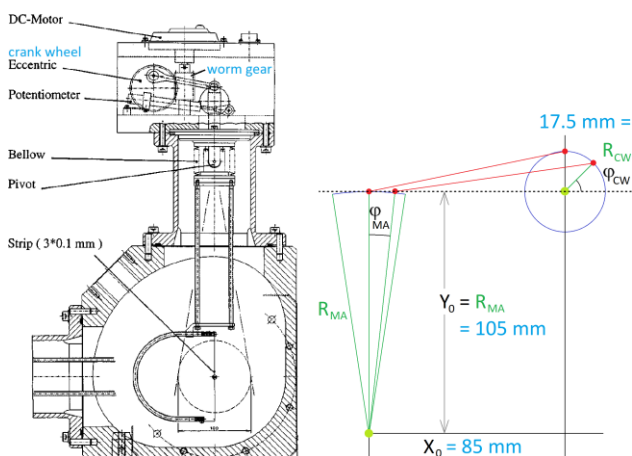

Figure 1: Present MA wire monitor. Wire crosses beam axis at $\varphi_{CW} = 90°$ and 270°. HS not shown. The monitor needs little space in beam direction. Horizontal and vertical MA are only 20 mm apart.

In the 0.87 MeV beam line and a few locations in the 72 MeV beam line, the power density at full proton beam current is too high to let the wire or foil survive at the given speed. Beam induced fluorescence monitors installed in 10 of 32 monitor locations in the 0.87 MeV line allow to

___
† doelling@protonmail.com, rudolf.doelling@psi.ch

measure at full beam current of 10 mA, however, with limited dynamic range. Wire monitors with at least approximately four times higher speed could be an alternative. By using a stepper motor instead of the DC motor, the potentiometer can be eliminated, and the control of the movement is simplified.

In the following we simulate the movement of variants of the present mechanics driven by stepper motors and conclude to wire speed and error of wire position caused by the motor characteristics.

MECHANICS

With the present monitor, the inertia of the 20:1 worm gear and the DC motor is high. We look at three alternatives with stepper motor and the same dimensions of CW-CR-MA connection (Fig. 1, right):

1. Only motor replaced. Worm gear reduction 20:1. The range of unidirectional CW movement is $\varphi_{CW} = 151.2°$ to 568.8°. The long travel allows a softer acceleration. Wire speed 0.75 m/s unchanged.
2. Whole mechanics replaced by a moderately less-inertia variant (Fig. 2c). No potentiometer. Spur gear reduction 3:1. Range $\varphi_{CW} = 151.2°$ to 568.8°. Wire speed 4 m/s.
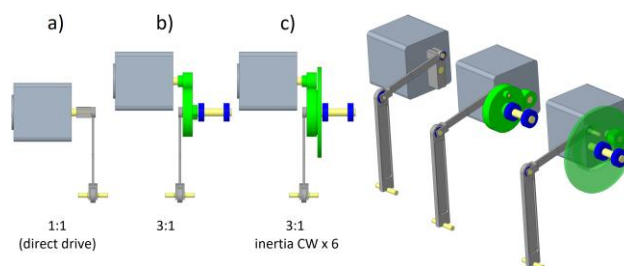3. Ditto, but gear reduction 1:1 (direct drive, Fig. 2a) and Range $\varphi_{CW} = 180°$ to 540°.

Figure 2: Lower-inertia setups (schematic).

In cases 2, 3, the wire position is determined by counting steps with respect to the HS switching positions. We assume a Baumer precision switch [3], pressed face on by the upper part of the MA. In order not to exceed the specification for the maximum approaching speed, the HS must be positioned not too far from the axis of rotation of the MA. Together with the play of the mechanism, this introduces a wire position error at beam axis of the order of 100 μm. Alternatively, the wire position can be determined by counting steps between the centres of the forward and backward measured beam profiles (if the beam has not shifted in between).

A brake is not needed. The MA is kept in the parking position against gravity by the CR, then in one line with the CW axis. Even the small holding torque of the currentless motor is sufficient for this.

SIMULATION PROCEDURE

Moments of inertia are estimated for motor, worm or spur MG or direct coupling, CW, CR and the complete MA. The masses of both halves of the CR are assumed to be concentrated in the connection points CW-CR and CR-MA. The actual MA angle is calculated from the CW angle analytically with the simplifying assumption that the connection point between CR and MA moves along the dotted line in Fig. 1 right.

The simulation is split into three runs, each done in time steps of $\Delta t = 0.2$ μs. In the <u>first run</u>, we define the 'preset trajectory' of the whole system by presetting over time one of the three 'input characteristics' a) rotor angular speed ω_{rot_pre}, b) rotor angular acceleration α_{rot_pre}, c) used fraction of pullout-torque $fracD_{pre}$. With the inertias, gear ratios, energy conservation (no losses are assumed in this run) and a preset dependency of pullout-torque on rotor angular speed $D_{pullout\_pre}(\omega_{rot})$, from each of the three 'input characteristics' a), b), c), the other two can be derived, together with the rotor angular position φ_{rot_pre} and the actual motor torque D_{pre} over time and many other parameters.

In the <u>second run</u>, the time dependent angular position of stator field and stator current phase $\varphi_{stat\_cur\_pre}$ is calculated via the phase difference $\varphi_{tooth\_pre} = \varphi_{stat\_cur\_pre} - \varphi_{rot\_pre}$, which results from the assumed 'cosine potential' condition $fracD_{pre} = \sin(\varphi_{tooth\_pre} \, n_{teeth})$, with n_{teeth} the number of teeth at the rotor. Optionally, $\varphi_{tooth\_pre} = 0$ can be used instead in this step ('φ_{tooth_pre} ignored'). However, this lack of adaptation will lead to significant deviations of the resulting trajectory from the 'preset trajectory', especially if these are not smooth as, e.g., the linear ramps often used.

Furthermore, the phase shift $\varphi_{diff\_induct\_pre}$ between stator voltage $\varphi_{stat\_volt\_pre}$ and stator current $\varphi_{stat\_cur\_pre}$ is calculated from the actual change of current, the inductance and resistance of stator coils and 50 m cable, and the available DC voltage (of the actual needed polarity).

(In this way, also the actual motor current could be calculated, which results in a sinusoidal time dependence for high DC voltage or low rotor angular speed, and in triangular time dependence for low DC voltage or high rotor angular speed. Integrating over a half period of same sign results in a charge which depends very similar on angular rotor speed as the pullout-torque given by the manufacturer, however with significant lower DC voltages than specified. We did not use this to calculate $D_{pullout\_pre}(\omega_{rot})$, but use the dependency given by the manufacturer.)

With this, we get the angular position of stator voltage $\varphi_{stat\_volt\_pre}$, i.e., the 'phase' set by the motor driver. It is changed not continuously, but, more realistic, only in full microsteps. To reproduce realistic driver properties, we assume that each microstep needs a minimum time of 2 μs. Further we assume $\varphi_{stat\_volt\_pre}$ is updated to the actual microstep only in time intervals corresponding to the pulse-width modulation (PWM) frequency $f_{PWM} = 40$ kHz of the driver.

Optionally, all microsteps corresponding to fullstep frequencies below, e.g., $f_{start,fs} = 500$ Hz can be suppressed.

This resembles the fullstep start frequency of linear ramps used in many drivers.

The <u>third run</u> starts from the microstep sequence represented by $\varphi_{stat\_volt\_pre}$. To this, a phase error is added, corresponding to the error of full-step positions due to manufacturing inaccuracies of the teeth of the rotor. The error is statistically distributed to the teeth within boundaries $\varphi_{err\_bound} = \pm 0.025°$. It is assumed that the error between one fullstep and the next changes linearly over half a fullstep. An offset is added to all errors to bring the error of the fullstep of the starting position to zero. In general, it is started at rest, hence this position is reached exactly.

φ_{diff_induct} is again calculated as above to get φ_{stat_cur}. From the difference φ_{tooth} to the actual φ_{rot} results the used fraction of pullout-torque $fracD = \sin(\varphi_{tooth} \, n_{teeth})$, and with the actual pullout-torque $k_{weak} \, D_{pullout}(\omega_{rot})$ we derive the torque D. Optionally, with k_{weak} different from 1, here 0.9, we account for the fact that the pullout-torque may differ from the specification.

The difference $d\varphi_{tooth}/dt$ of angular speeds of stator current ω_{stat_cur} and rotor ω_{rot} causes a viscous drag, leading to a torque $D_{loss} = h_{loss} \, d\varphi_{tooth}/dt$, which leads to a damping of eventual oscillations of the rotor angular position in the 'cosine potential' of the teeth (OICP). $h_{loss} = 0.003$ Js/rad^2 is roughly estimated from the damping of oscillations after a single step starting from rest. Optionally, no damping can be assumed. (Microsteps are assumed to instantaneously change φ_{tooth}, not slowed by inductance, which is taken into account only summarily via φ_{diff_induct}. In time steps, where a microstep is executed, this leads to unrealistic large values of D_{loss}, depending on the length of time steps. This cancels out over a microstep and is not critical for the overall trajectory. For a decent plotting, depending parameters are averaged over a microstep or fullstep. Only every 1000th time step is plotted.)

With the inertias, gear ratios, energy conservation and $D_{pullout}(\omega_{rot})$, from the total torque, the change $d\varphi_{rot}/dt$ is calculated, and from this the positions, speeds and kinetic energies of all the other parts and the torques between them, i.e., the 'resulting trajectory' of the system. In this part, an efficiency η_{gear} of the gear between motor and CW can be considered, which is useful in the case of a worm gear. (This option cannot be used together with D_{loss}, since its momentarily unrealistic large values would not cancel out and would cause an unrealistic large overall gear loss.)

In the resulting trajectory, OICP are visible. This is more prominent in the rotor angular speed and acceleration, $fracD$, and other parameters. The excitation is caused by the '<u>disturbing conditions</u>' introduced above (<u>printed in blue</u>), but also by not well adapted 'input characteristics', especially if in the second run, φ_{tooth_pre} is ignored.

Further parameters of the trajectory are calculated, as position x_{wire}, speed v_{wire} and acceleration a_{wire} of the wire at the height of the beam, the wire position increment dx_{wire} corresponding to a fullstep, the deviation $x_{wire\_dev2pre}$ of wire position against the preset trajectory, and also $x_{wire\_dev2pre\_corr}$, the same corrected for the predictable part of the effects of PWM and, in case, ignoring φ_{tooth_pre}.

12th Int. Beam Instrum. Conf.   IBIC2023, Saskatoon, Canada   JACoW Publishing

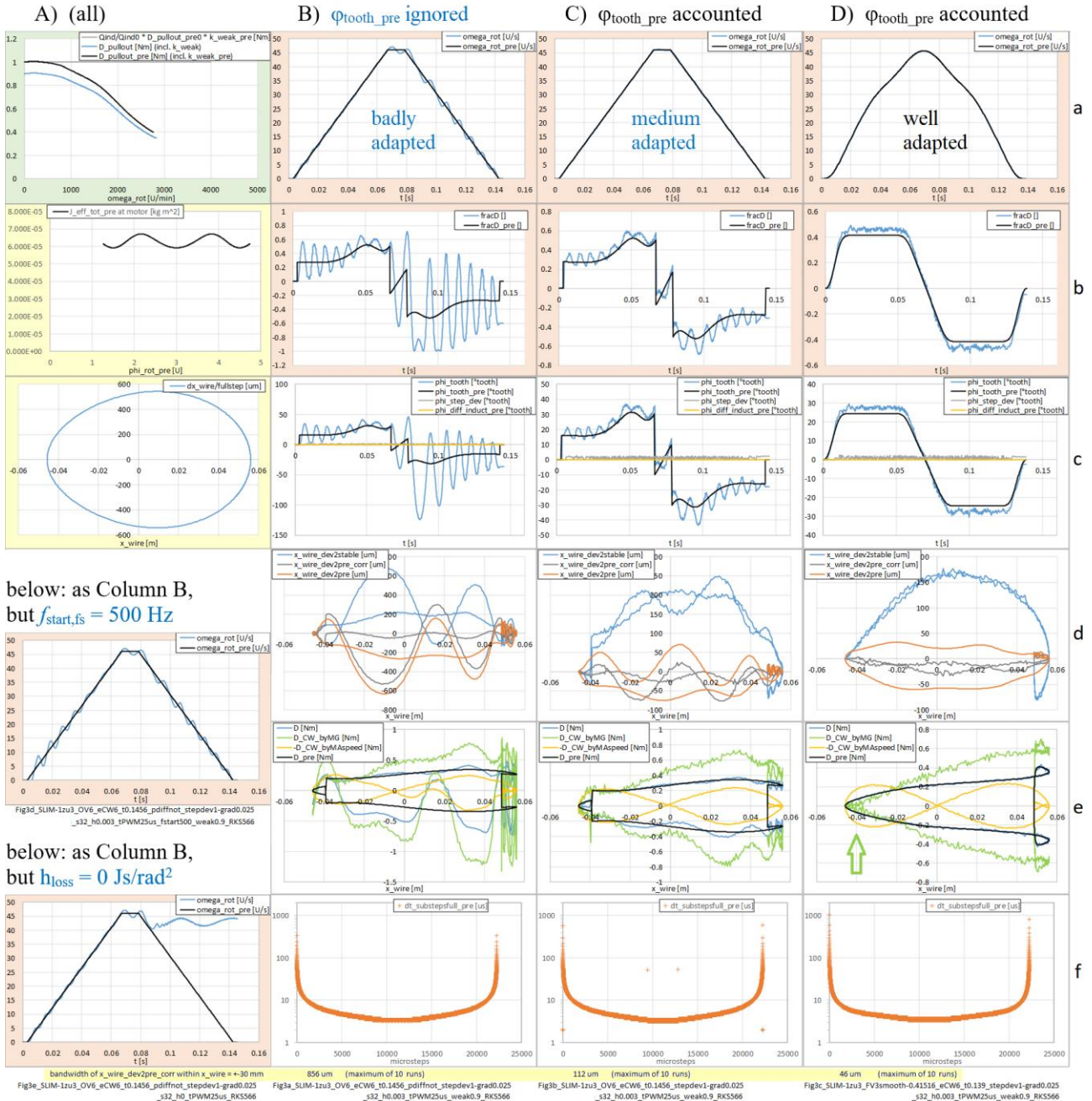ISBN: 978-3-95450-236-3   ISSN: 2673-5350   doi:10.18429/JACoW-IBIC2023-WEP018

SIMULATION RESULTS

Figure 3: Case 2: Spur gear reduction 3:1, 50 motor teeth, $h_{loss} = 0.003$ Js/rad^2, $f_{start,fs} = 0$ Hz, 6400 microsteps/revolution, $\varphi_{err\_bound} = \pm0.025°$, $f_{PWM} = 40$ kHz, $k_{weak} = 0.9$. Column A: a) Pullout-torque characteristic, only used part shown (black: preset trajectory, blue: resulting trajectory), b) total inertia seen by the motor, c) wire position change per fullstep depending on wire position. Column B, C, D: a) Rotor speed over time, b) used fraction of actual pullout-torque, c) phase in 'cosine potential' (grey: deviation due to manufacturing inaccuracies, yellow: due to inductance), d) deviation of wire position (red: to preset trajectory, grey: ditto, corrected, blue: compared to bottom of 'cosine potential'), e) torques of motor and at CW due to MG (green) and MA (yellow). Due to the larger CW inertia (Fig. 2c versus 2b), the torque D_{CW_byMG} of CW to MG changes its sign distant from the beam axis (arrow), thereby minimizing the effect of gear play to the measured profile shape at Column C, D. f) Preset step sequence (time difference between microsteps). At Column C the few adapted microstep intervals at the limits of the ramps are visible. Columns B, C, D present simulations for different input characteristics, ranging from 'badly adapted' to 'well adapted'. The two variants at bottom left illustrate that it depends on details, how 'badly adapted' input characteristics interfere with the eigenfrequency of OICP. This is less critical with 'well adapted' smooth input characteristics.
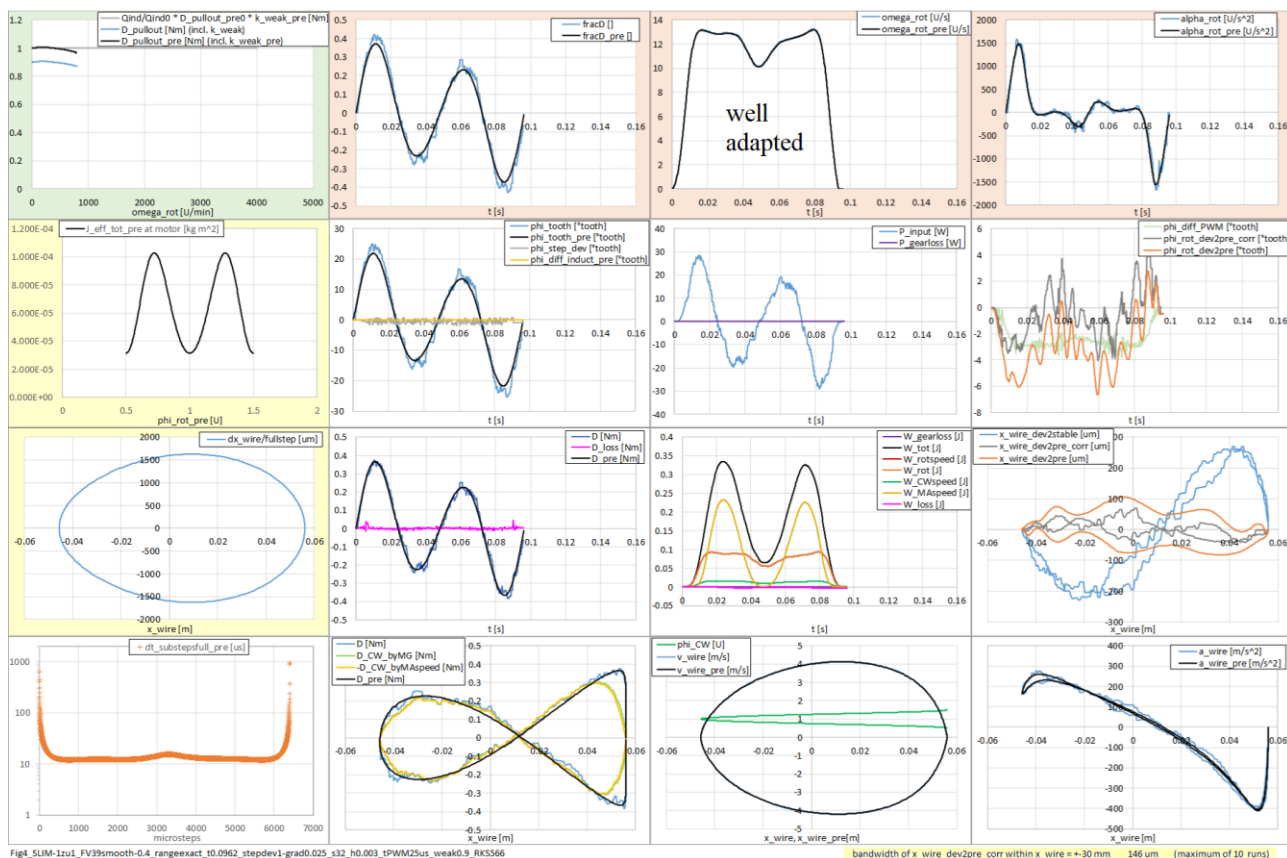
Figure 4: Case 3: Direct drive 1:1. Parameters as in Fig. 3 caption. Additional information compared to Fig. 3: Rotor acceleration, motor power, deviations of rotor phase by PWM (green) and against preset (red) and ditto corrected (grey), energies of parts of the mechanism, wire velocity and CW angular position, wire acceleration.

The example of case 2 (Fig. 3) and further simulations imply that OICP are reduced by (in this order)

- taking into account $\varphi_{\text{tooth\_pre}}$
- providing a (preferentially smooth) input characteristic, not interfering with the eigenfrequency of OICP
- the presence of damping $h_{\text{loss}} > 0$ Js/rad^2
- microstepping at least at lower speeds
- small other disturbing conditions
- reduced motor current, if torque is abundant.

Thereby the accuracy of wire movement is improved, and the used fraction of pullout-torque reduced.

With an adapted input characteristic and parameters assumed to be realistic, the simulations suggest that for cases 2 and 3 (Fig. 4), a wire speed of 4 m/s is well in reach. Electronics able to provide a microstep sequence from a look-up table to the step-direction input of a commercial driver is required for this. The predicted accuracy of wire movement, defined as band width of $x_{\text{wire\_dev2pre\_corr}}$, is somewhat better at gear ratio 3:1 (~50 μm) than at 1:1 (~150 μm). With lower wire velocity the accuracy does not improve. Here, a higher gear ratio can provide better accuracy. With 20:1 (case 1) ~3 μm is predicted, which is smaller than the effect of the to be expected mechanical play of the mechanism.

An ultimate limit for maximum wire speed is given by the available motor torque. However, OICP will lead to a loss of synchronisation already at somewhat lower speeds. This is described by the simulation (Fig. 3 bottom left). For quantitative predictions, at least, a more precise determination of h_{loss} is required. Experimental tests are needed to check the predictions of the simulation. A simple test case can be a motor loaded with an additional inertia.

OUTLOOK

A test stand is under preparation [4] to evaluate the performance of monitor setups as the ones discussed here. Furthermore, other aspects, as the lifetime of the bellows, the stiffness of the MA and wire vibrations will be studied.

ACKNOWLEDGEMENTS

REFERENCES

[1] L. Rezzonico, "Beam diagnostics at SIN", in *Proc. CYCLO-TRONS'86*, Tokyo, Japan, Oct. 1986, paper I5-05, pp. 457-460.

[2] L. Rezzonico, M. Olivo, "Profile measurements of high intensity-low energy ion beams", *Rev. Sci. Instrum.*, vol. 67, no. 3, pp. 1246-1248, 1996.
doi:10.1063/1.1146687

[3] https://www.baumer.com

[4] Stuart Warren, PSI, personal communication.